Paper:
Zhao, Y., Al Abass, N., Malpass-Evans, R., Carta, M., McKeown, N., Madrid, E., Fletcher, P. & Marken, F. (2019). Photoelectrochemistry of immobilised Pt@g-C3N4 mediated by hydrogen and enhanced by a polymer of intrinsic microporosity PIM-1. *Electrochemistry Communications, 103*, 1-6.
http://dx.doi.org/10.1016/j.elecom.2019.04.006

Electrochemistry Communications 103 (2019) 1–6

Contents lists available at ScienceDirect

Electrochemistry Communications

journal homepage: www.elsevier.com/locate/elecom

Short communication

Photoelectrochemistry of immobilised Pt@g-C_3N_4 mediated by hydrogen and enhanced by a polymer of intrinsic microporosity PIM-1

Yuanzhu Zhao[a], Nawal Abdullah Al Abass[b], Richard Malpass-Evans[c], Mariolino Carta[d], Neil B. McKeown[c], Elena Madrid[a], Philip J. Fletcher[e], Frank Marken[a,*]

[a] Department of Chemistry, University of Bath, Claverton Down, Bath BA2 7AY, UK
[b] KACST, PO Box 6086, Riyadh 11442, Saudi Arabia
[c] School of Chemistry, University of Edinburgh, Joseph Black Building, West Mains Road, Edinburgh, Scotland EH9 3JJ, UK
[d] Department of Chemistry, Swansea University, College of Science, Grove Building, Singleton Park, Swansea SA2 8PP, UK
[e] Materials and Chemical Characterisation Facility (MC^2), University of Bath, Claverton Down, BA2 7AY, UK

ARTICLE INFO

Keywords:
Nanomaterials
Photovoltammetry
Electroanalysis
Photovoltaics
Photo-synthesis
Glucose

ABSTRACT

Graphitic carbon nitride with photo-attached platinum nanoparticles of typically 2.5 nm diameter, Pt@g-C_3N_4, is known for photo-generation of hydrogen in aqueous environments and in the presence of hole quenchers. Here, the generation of photocurrents from photo-hydrogen production is observed at a platinum electrode, driven by oxalate or glucose hole quenchers, and enhanced with a polymer of intrinsic microporosity PIM-1 coated over the Pt@g-C_3N_4 deposit. The ability of PIM-1 to create triphasic conditions and to capture hydrogen leads to enhanced photocurrent responses, even in the presence of ambient oxygen. Effects are discussed in terms of triphasic solid|liquid|hydrogen gas-based electrode processes. A glucose-concentration-dependent (super-Langmuirian) photo-response is observed. Possible applications are proposed in glucose sensing and in hydrogen-mediated photovoltaics.

1. Introduction

Photoelectrochemical processes generally rely on excitation of a photoabsorber followed by charge separation and transport of charges. In particular, systems have been developed based on porous semiconductor electrodes, e.g. Grätzel cells [1]. However, charge carrier transport could be replaced by other types of energy carrier transport mechanisms. It is shown here for the case of the graphitic carbon nitride photocatalyst, g-C_3N_4, that the mobile species in a photoelectrochemically active device can also be neutral, based on hydrogen diffusion. The efficiency for hydrogen capture and transport towards the photo-electrode surface is enhanced under triphasic reaction conditions with a microporous polymer film coating.

The photocatalyst graphitic carbon nitride, g-C_3N_4, has been known for many years [2,3] and is readily prepared [4,5] from organic precursors. This type of catalyst has been shown to be effective in light-driven water splitting even in pure water [6] without added quencher molecules. Graphitic carbon nitride absorbs light in the blue up to approximately 450 nm with a band gap of 2.7 eV [7]. Catalysts can be deposited onto the particulate g-C_3N_4 (obtained from melamine [8]) to enhance charge separation and water splitting reactions. Nanoparticulate platinum photo-deposited onto particulate g-C_3N_4 (to give Pt@g-C_3N_4 [9]) is known to result in good hydrogen evolution characteristics [10,11]. In this report, particulate Pt@g-C_3N_4 photocatalyst is coated onto a platinum working electrode to give a new type of photo-active electrode. In contrast to traditional semiconductor electrodes that are based on charge carrier transport, hydrogen is produced locally (as energy carrier) and transported to the electrode surface. This type of process is shown to be enhanced by coating with a hydrogen-capture film based on a polymer of intrinsic microporosity PIM-1 [12,13].

Polymers of intrinsic microporosity (PIMs) have been introduced to electrochemistry only relatively recently [14,15]. Beneficial features of PIMs include ease of processing from solution, a molecularly rigid structure creating a high surface area, and porosity with pores typically 1–2 nm in size. The effects of polymers of intrinsic microporosity on triphasic solid|liquid|gas catalytic reactions have been noted previously, for example in oxygen reduction and hydrogen evolution [16], in formic acid oxidation [17], and in hydrogen gas transport in partially carbonised PIM materials with embedded platinum catalysts [18]. PIM-1 has the ability to allow electrolyte transport whilst simultaneously binding and transporting hydrogen gas. Fig. 1 shows the molecular

* Corresponding author.
E-mail address: f.marken@bath.ac.uk (F. Marken).

https://doi.org/10.1016/j.elecom.2019.04.006
Received 30 March 2019; Received in revised form 6 April 2019; Accepted 9 April 2019
Available online 10 April 2019

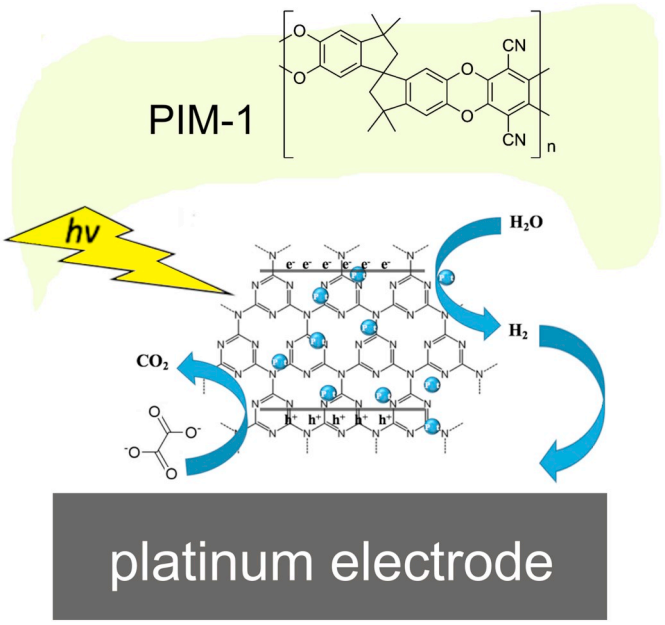

Fig. 1. Schematic illustration of Pt@g-C_3N_4 photocatalyst at a platinum electrode surface generating hydrogen. A PIM-1 coating is applied to provide mechanical stability, to capture hydrogen, and to provide triphasic reaction conditions.

structure of PIM-1 and a schematic illustration of a process in which light-induced hydrogen evolution occurs close to the electrode surface with a layer of PIM-1 providing mechanical stability and a hydrogen capture function.

In this exploratory study, the effects of PIM-1 coatings on the performance of Pt@g-C_3N_4 photocatalyst are investigated for light-driven hydrogen evolution processes. Quenchers such as oxalate and glucose are investigated. Oxalate is a well-known and very effective quencher and employed here at high concentration to maximise the hole-quenching effect. Glucose has been selected as a model saccharide and as a potential break-down product of biomass. Photocurrents are generated even in the presence of ambient oxygen. A correlation of photocurrent with glucose concentration is demonstrated and a mechanism is proposed, comparing argon de-aerated and ambient oxygen conditions.

2. Experimental

2.1. Reagents

PIM-1 was prepared following a literature procedure [19,20]. A solution of 2 mg PIM-1 in 1 mL chloroform (see Fig. 2d) was applied to electrode surfaces. The photocatalyst g-C_3N_4 was obtained by heating melamine in a closed but gas-exchanging ceramic boat (500 °C, 3 h) adopting a literature methodology [9,21]. Platinum nanoparticles were photo-attached to the photocatalyst by stirring a suspension of the photocatalyst in 0.3 M di-sodium oxalate with illumination (LED, λ = 385 nm, approximately 100 mW cm^{-2}) for 72 h. A grey colour (Fig. 2e) clearly indicated the presence of platinum metal. Energy dispersive X-ray analysis (EDX) confirmed the presence of platinum in the form of nanoparticles, typically 2.5 nm in diameter (see Fig. 2c).

2.2. Instrumentation

Electrochemical experiments were performed with an Autolab PGSTAT (Metrohm, UK) controlling a three-electrode system with a 3 mm diameter platinum working electrode, a saturated calomel SCE reference electrode, and a platinum wire counter electrode. The

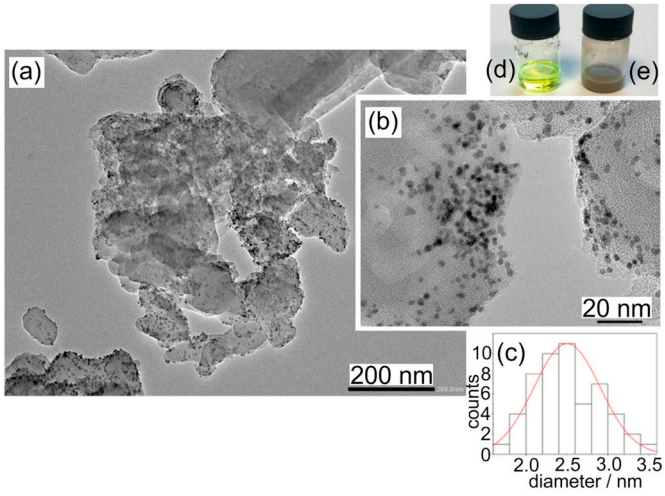

Fig. 2. (a, b) Characterisation of Pt@g-C_3N_4 with TEM. (c) Histogram of the platinum nanoparticle size distribution with a maximum at diameter 2.5 nm. Photographic images of (d) PIM-1 solution in chloroform and (e) of the Pt@g-C_3N_4 suspension in isopropanol.

electrochemical cell allowed light from a power LED (λ = 385, Thorlabs, UK) to pass through a quartz window and 2 ± 1 mm solution to interact with the working electrode. Transmission electron microscopy (TEM) images were obtained with a JEOL JEM-2100Plus system equipped with an Oxford Instruments X-Max^N TSR Windowless Energy dispersive X-ray analyser (EDX).

3. Results and discussion

3.1. Photoelectrochemical hydrogen evolution at Pt@g-C_3N_4 enhanced by PIM-1: oxalate quencher

Initially, a quencher solution of saturated sodium oxalate (approximately 0.3 M di-sodium oxalate at pH = 7.4) is employed to generate substantial photocurrents. 75 µg Pt@g-C_3N_4 is deposited onto a 3 mm diameter platinum disk working electrode and is then immersed into the quencher solution in line with the LED light source. Fig. 3A shows a cyclic voltammogram with a prominent reduction peak at −0.1 V vs. SCE (black line). This can be identified as the reduction of ambient oxygen. When applying pulses of light (LED, 385 nm, ca. 100 mW cm^{-2}, 2 s on and 1 s off, red line) clear oxidation responses are detected due to the localised formation of hydrogen at the Pt@g-C_3N_4 photocatalyst. The hypothetical mechanism can be expressed as a sequence of excitation (Eq. (1)), charge separation (Eq. (2)), hole quenching (Eq. (3)), hydrogen evolution (Eq. (4)) in competition with oxygen reduction, and hydrogen consumption (Eq. (5)) at the platinum working electrode.

$$\text{Pt@g} - C_3N_4 + h\nu \rightarrow \text{Pt@g} - C_3N_4^* \quad (1)$$

$$\text{Pt@g} - C_3N_4^* \rightarrow \text{Pt}^-\text{@g} - C_3N_4^+ \quad (2)$$

$$\text{Pt}^-\text{@g} - C_3N_4^+ + ½\ \text{oxalate}^{2-} \rightarrow \text{Pt}^-\text{@g} - C_3N_4 + CO_2 \quad (3)$$

$$\text{Pt}^-\text{@g} - C_3N_4 + H^+ \rightarrow ½\ H_2 \quad (4)$$

$$H_2 \rightarrow 2H^+ + 2\ e^-(\text{platinum}) \quad (5)$$

When this experiment is repeated under the same conditions, but after de-aeration with argon, the oxygen reduction peak is removed (see Fig. 3B, black line) and the photocurrent signals are increased over the complete range of applied potentials. Now, in the presence of light, the oxidation of hydrogen produces a threefold increase in photocurrents (close to 17 µA). The presence of recombination processes due to oxygen, evident in data in Fig. 3A, has been eliminated. Next, the

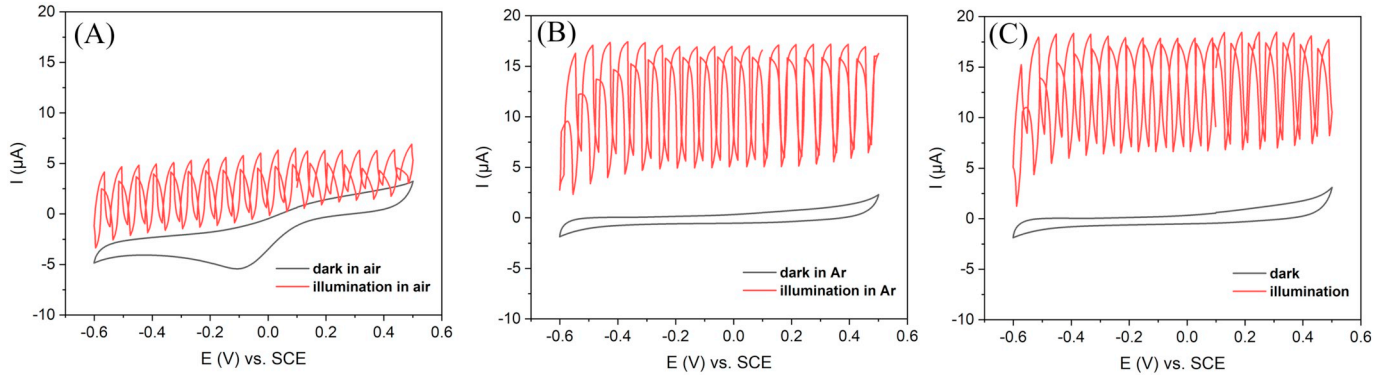

Fig. 3. Cyclic voltammograms (scan rate 20 mV s^{-1}; black = no illumination; red = 2 s on and 1 s off, 385 nm LED) at a 3 mm diameter platinum disk electrode coated with Pt@g-C_3N_4 and immersed in 0.3 M di-sodium oxalate; (A) in ambient air with 75 μg Pt@g-C_3N_4. (B) under argon with 75 μg Pt@g-C_3N_4; (C) under argon with 150 μg Pt@g-C_3N_4. (For interpretation of the references to colour in this figure legend, the reader is referred to the web version of this article.)

experiment is repeated with a higher loading of photocatalyst (150 μg). Fig. 3C shows that the effect of doubling the amount of photocatalyst on the voltammetric responses is minor and that therefore the loading with catalyst is not a crucial experimental parameter.

A polymer of intrinsic microporosity PIM-1 can be employed to capture hydrogen and to modify the local reaction conditions at the electrode surface. When applying the polymer PIM-1 over the surface of the photocatalyst, significant changes in photocurrents can be observed. In Fig. 4, data are shown for argon deaerated oxalate solution and for (A) no PIM-1, (B) 10 μg PIM-1, and (C) 20 μg PIM-1. The presence of the PIM-1 polymer almost doubles the photocurrents, which can be attributed to hydrogen being captured and concentrated in the PIM-1 film. Hydrogen is then preferentially guided to the platinum electrode surface rather than escaping into the solution. Data in Fig. 4C show further improvements with a thicker film of PIM-1. In fact, an underlying increase in apparent background current can also be attributed to the presence/build-up of hydrogen. It is interesting to note that the onset potential for hydrogen evolution is shifted in a positive direction in the presence of additional PIM-1 (see Fig. 4B and C). This is linked to the local formation of protons during hydrogen oxidation at the platinum electrode. Acidification within the Pt@g-C_3N_4 catalyst layer is more likely with a thicker PIM-1 coating and as a result the onset potential for hydrogen oxidation is shifted in a positive direction (see Fig. 4C and F).

Next, this experiment is repeated but without de-aeration with argon. Fig. 4D shows data for 75 μg Pt@g-C_3N_4 in 0.3 M disodium oxalate. When a film of PIM-1 is applied (Fig. 4E) a substantial increase in current is observed. Doubling the PIM-1 layer thickness (Fig. 4F) further

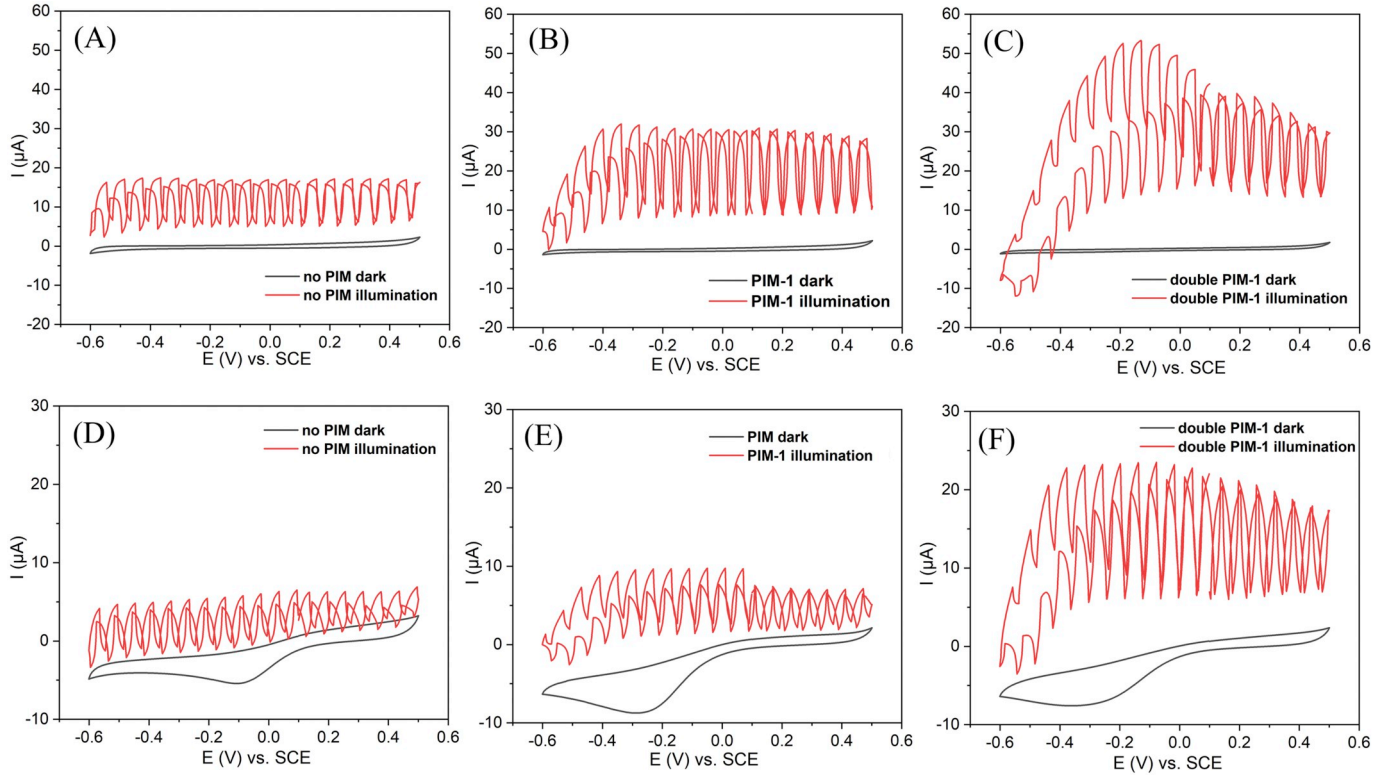

Fig. 4. Cyclic voltammograms (scan rate 20 mV s^{-1}; black = no illumination; red = 2 s on and 1 s off, 385 nm LED) at a 3 mm diameter platinum disk electrode coated with Pt@g-C_3N_4 and immersed in 0.3 M disodium oxalate; (A) under argon with 75 μg Pt@g-C_3N_4; (B) as before with 10 μg PIM-1; (C) as before with 20 μg PIM-1; (D) in ambient air with 75 μg Pt@g-C_3N_4; (E) as before with 10 μg PIM-1; (F) as before with 20 μg PIM-1. (For interpretation of the references to colour in this figure legend, the reader is referred to the web version of this article.)

improves the photocurrent responses.

3.2. Photoelectrochemical hydrogen evolution at Pt@g-C_3N_4 enhanced by PIM-1: glucose quencher

Glucose is a reducing carbohydrate and readily oxidised at approximately 0.15 V–0.3 V vs. RHE (reversible hydrogen electrode) with a suitable catalytic electrodes including platinum [22]. Holes generated during illumination of g-C_3N_4 are therefore quenched (see Eq. (9)) to increase the formation of hydrogen. However, competition to oxygen evolution (Eq. (8)) may also be possible.

$$Pt@g - C_3N_4 + h\nu \rightarrow Pt@g - C_3N_4^* \quad (6)$$

$$Pt@g - C_3N_4^* \rightarrow Pt^-@g - C_3N_4^+ \quad (7)$$

$$Pt^-@g - C_3N_4^+ + \tfrac{1}{2}\, H_2O \rightarrow Pt^-@g - C_3N_4 + \tfrac{1}{2}\, O_2 + H^+ \quad (8)$$

$$Pt^-@g - C_3N_4^+ + \tfrac{1}{2}\, H_2O + \tfrac{1}{2}\, \text{glucose} \rightarrow Pt^-@g - C_3N_4 + \tfrac{1}{2}\, \text{gluconate} + H^+ \quad (9)$$

$$Pt^-@g - C_3N_4 + H^+ \rightarrow \tfrac{1}{2}\, H_2 \quad (10)$$

$$H_2 \rightarrow 2H^+ + 2\, e^-(\text{platinum}) \quad (11)$$

Fig. 5A shows data for a solution of 0.1 M glucose in 0.1 M NaOH in contact with a Pt@g-C_3N_4 modified electrode (75 µg photo-catalyst deposit). In the cyclic voltammogram without illumination (black line) some oxidation of glucose occurs. When employing pulsed LED light (red line) anodic photocurrent pulses consistent with hydrogen production are observed. These current pulses are diminished at a potential positive of 0.0 V vs. SCE due to oxygen interference. At potentials negative of 0.0 V vs. SCE, oxygen is consumed directly at the Pt working electrode and photocurrents increase. When applying a film of PIM-1 (10 µg; Fig. 5B), photocurrents increase and show less dependence on the applied potential. When increasing the concentration of glucose to 0.5 M (Fig. 5C), a further increase in photocurrent is noted. With additional PIM-1 (30 µg; Fig. 5D) the photocurrent is further improved. However, the rise time and decay time for these photocurrents is now relatively slow. Therefore, additional experiments are performed for a longer time in chronoamperometry mode and over a wider range of glucose concentrations.

Fig. 6 shows data for light-on and light-off current responses for 75 µg Pt@g-C_3N_4 catalyst coated with 30 µg PIM-1. It can be seen that the photocurrent increases with glucose concentration. However, on reaching concentrations of 1.0 M and higher the increase is less pronounced and a plateau region is observed. This can be understood in terms of glucose adsorption onto the Pt@g-C_3N_4 photocatalyst and saturation of the photocatalyst surface at very high glucose concentrations. A plot of the photocurrent data versus glucose concentration is shown in Fig. 6B with the "ideal" line for a Langmuirian glucose

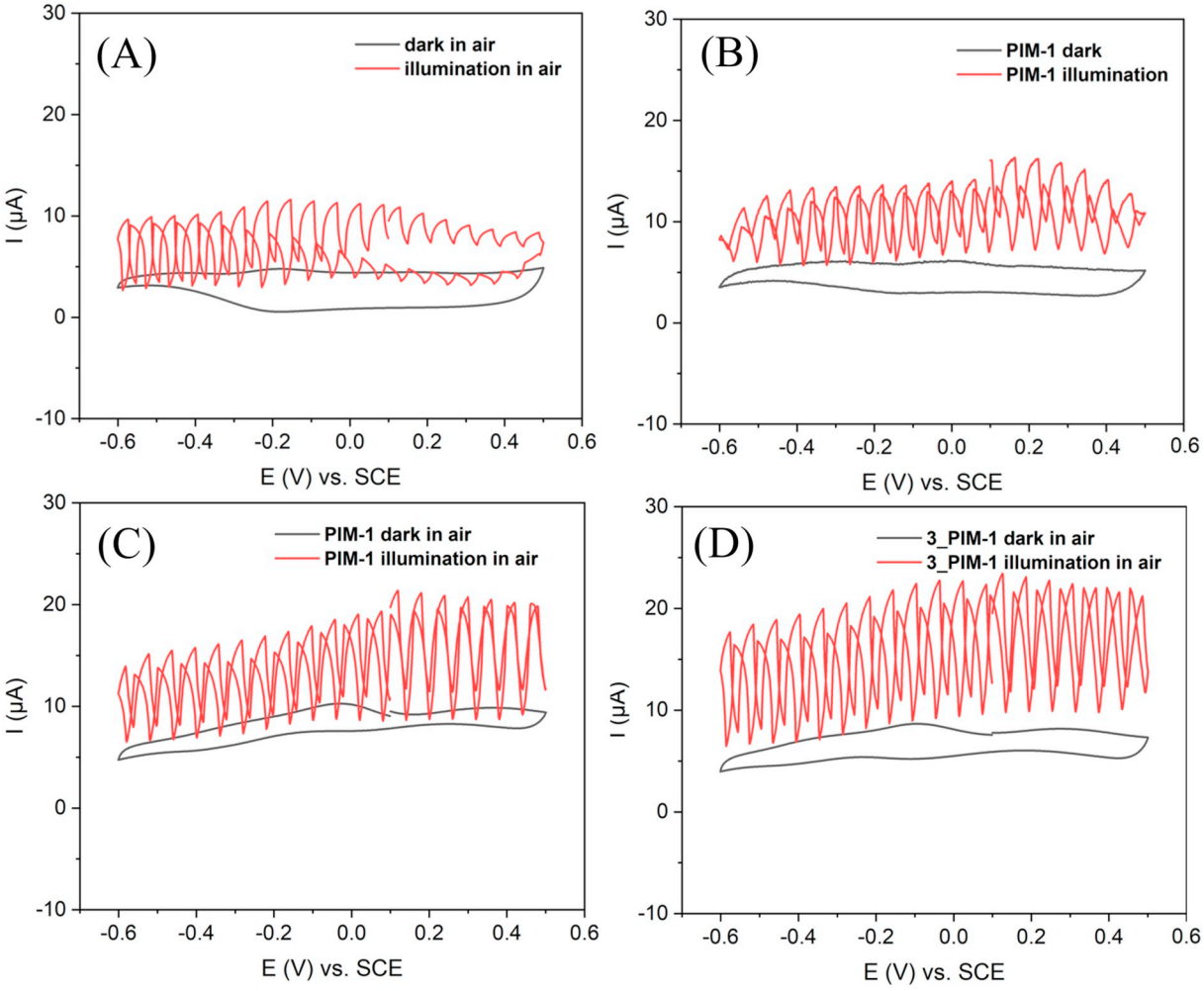

Fig. 5. Cyclic voltammograms (scan rate 20 mV s^{-1}; black = no illumination; red = 2 s on and 1 s off, 385 nm LED) at a 3 mm diameter platinum disk electrode coated with Pt@g-C_3N_4 and immersed in 0.1 M NaOH; (A) 0.1 M glucose in ambient air with 75 µg Pt@g-C_3N_4; (B) as before with 10 µg PIM-1; (C) 0.5 M glucose in ambient air with 75 µg Pt@g-C_3N_4 with 10 µg PIM-1; (D) as before with 30 µg PIM-1. (For interpretation of the references to colour in this figure legend, the reader is referred to the web version of this article.)

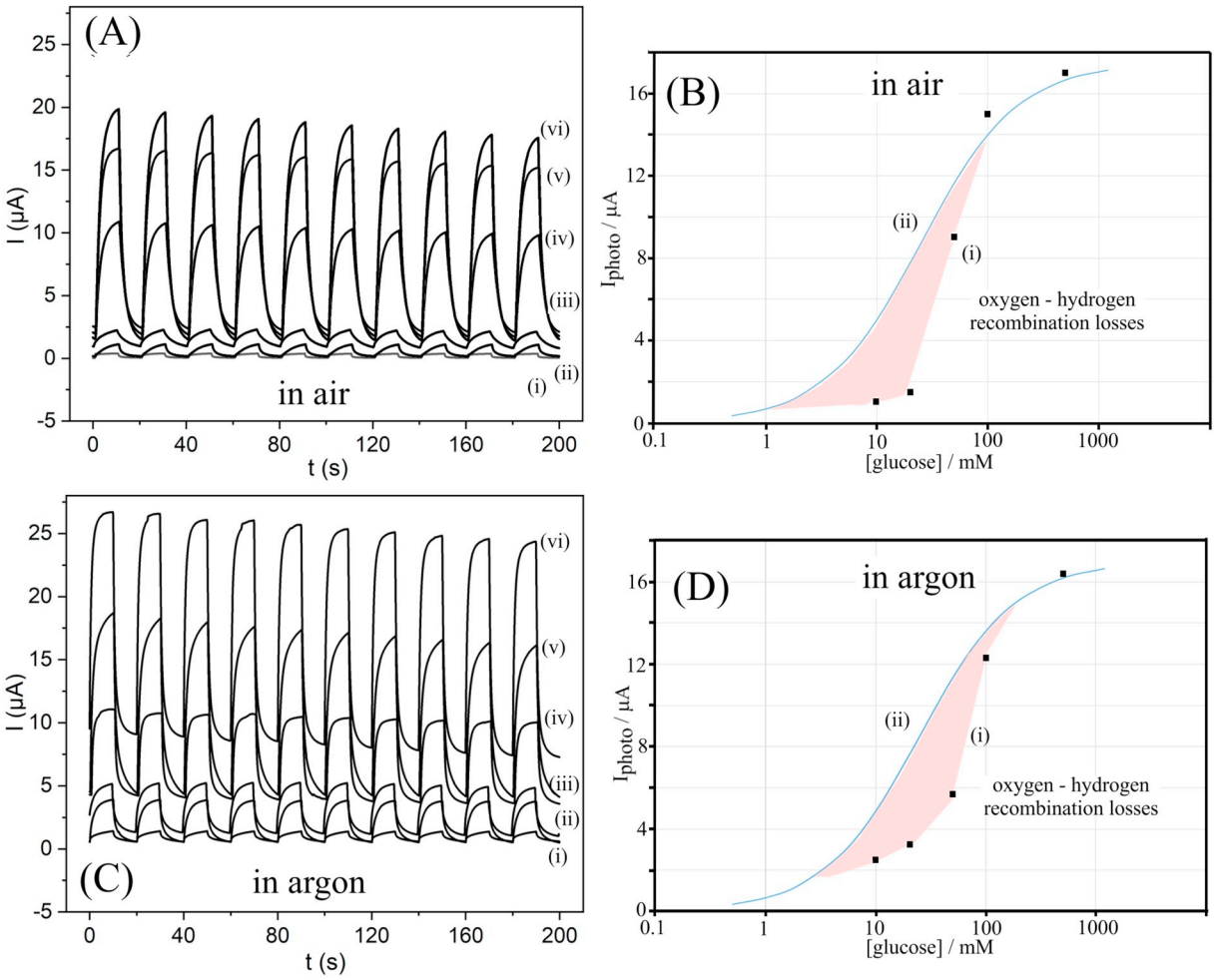

Fig. 6. (A) Chronoamperometry data (0.0 V vs. SCE; 10 s on and 10 s off, 385 nm LED) at a 3 mm diameter platinum disk electrode coated with Pt@g-C_3N_4 with 30 μg PIM-1 and immersed in 0.1 M NaOH with (i) 0.0, (ii) 10, (iii) 20, (iv) 50, (v) 100, and (vi) 500 mM glucose in ambient air with 75 μg Pt@g-C_3N_4. (B) Plot of photocurrent versus glucose concentration with a line indicating the Langmuir model with binding constant 40 mol^{-1} dm^3. (C) As above but under argon. (D) Plot of photocurrents versus glucose concentration with a line indicating the Langmuir model with binding constant 40 mol^{-1} dm^3.

adsorption (with a binding constant $K_{Langmuir}$ = 40 mol^{-1} dm^3) included. The deviation from the Langmuir binding model suggests a recombination pathway at lower glucose concentrations. Oxygen is known to quickly react with hydrogen (at the Pt catalyst). Therefore, further experiments were performed under argon with very similar results (Fig. 6C and D). It is therefore proposed that incomplete adsorption coverage with glucose at the Pt@g-C_3N_4 surface may lead to localised oxygen formation (see Eq. (8)) and this could be responsible for additional recombination losses at lower quencher concentration and super-Langmuirian characteristics. However, there could be other/additional mechanisms (e.g. interaction of glucose with platinum) giving rise to similar phenomena and further work will be required to investigate this process in more detail.

4. Conclusions and outlook

It has been shown that photoelectrochemical hydrogen evolution at Pt@g-C_3N_4 catalyst particles occurs in aqueous environments enhanced by hole quenchers. With a film coating of a polymer of intrinsic microporosity PIM-1, the hydrogen product can be accumulated close to the electrode to give more substantial photocurrents.

The photocurrents are shown to provide an analytical measure for the concentration of glucose in aqueous solution. Adsorption of glucose is proposed and (at lower glucose concentrations) the competing formation of oxygen may result in a super-Langmuirian dependency. More work will be required to further develop the analytical application (e.g. for different carbohydrates) as well as to improve the insight into the mechanism for a wider range of hole quenchers and conditions.

Acknowledgements

Y.Z. thanks the China Scholarship Council (CSC scholarship No 20180935006) for a PhD scholarship. E.M. and F.M. thank EPSRC for support (EP/N013778/1).

References

[1] L.M. Peter, J. Phys. Chem. Lett. 2 (2011) 1861–1867.
[2] J.Q. Wen, J. Xie, X.B. Chen, X. Li, Appl. Surf. Sci. 391 (2017) 72–123.
[3] G.P. Dong, Y.H. Zhang, Q.W. Pan, J.R. Qiu, J. Photochem. Photobiol. C: Photochem. Rev. 20 (2014) 33–50.
[4] Z.X. Zhou, Y.Y. Zhang, Y.F. Shen, S.Q. Liu, Y.J. Zhang, Chem. Soc. Rev. 47 (2018) 2298–2321.
[5] F.L. Wang, Y.P. Feng, P. Chen, Y.F. Wang, Y.H. Su, Q.X. Zhang, Y.Q. Zeng, Z.J. Xie, H.J. Liu, Y. Liu, W.Y. Lv, G.G. Liu, Appl. Catal. B Environ. 227 (2018) 114–122.
[6] G.G. Zhang, Z.A. Lan, L.H. Lin, S. Lin, X.C. Wang, Chem. Sci. 7 (2016) 3062–3066.
[7] F. Dong, Z.W. Zhao, T. Xiong, Z.L. Ni, W.D. Zhang, Y.J. Sun, W.-K. Ho, ACS Appl. Mater. Interfaces 5 (2013) 11392–11401.
[8] S.C. Yan, Z.S. Li, Z.G. Zou, Langmuir 25 (2009) 10397–10401.
[9] M.J. Liu, P.F. Xia, L.Y. Zhang, B. Cheng, J.G. Yu, ACS Sustain. Chem. Eng. 6 (2018) 10472–10480.
[10] F. Fina, H. Ménard, J.T.S. Irvine, Phys. Chem. Chem. Phys. 17 (2015) 13929–13936.
[11] S.W. Cao, J. Jiang, B.C. Zhu, J.G. Yu, Phys. Chem. Chem. Phys. 18 (2016) 19457–19463.

[12] P.M. Budd, N.B. McKeown, B.S. Ghanem, K.J. Msayib, D. Fritsch, L. Starannikova, N. Belov, O. Sanfirova, Y. Yampolskii, V. Shantarovich, J. Membr. Sci. 325 (2008) 851–860.
[13] Z.X. Low, P.M. Budd, N.B. McKeown, D.A. Patterson, Chem. Rev. 118 (2018) 5871–5911.
[14] F.J. Xia, M. Pan, S.C. Mu, R. Malpass-Evans, M. Carta, N.B. McKeown, G.A. Attard, A. Brew, D.J. Morgan, F. Marken, Electrochim. Acta 128 (2014) 3–9.
[15] E. Madrid, N.B. McKeown, Curr. Opin. Electrochem. 10 (2018) 61–66.
[16] E. Madrid, J.P. Lowe, K.J. Msayib, N.B. McKeown, Q.L. Song, G.A. Attard, T. Düren, F. Marken, ChemElectroChem 6 (2019) 252–259.
[17] A. Mahajan, S.K. Bhattacharya, S. Rochat, A.D. Burrows, P.J. Fletcher, Y.Y. Rong, A.B. Dalton, N.B. McKeown, F. Marken, ChemElectroChem (2019), https://doi.org/10.1002/celc.201801359.
[18] R.K. Adamik, N. Hernández-Ibáñez, J. Iniesta, J.K. Edwards, A.G.R. Howe, R.D. Armstrong, S.H. Taylor, A. Roldan, Y.Y. Rong, R. Malpass-Evans, M. Carta, N.B. McKeown, D.P. He, F. Marken, Nanomaterials 8 (2018) 542.
[19] P.M. Budd, E.S. Elabas, B.S. Ghanem, S. Makhseed, N.B. McKeown, K.J. Msayib, C.E. Tattershall, D. Wang, Adv. Mater. 16 (2004) 456–457.
[20] P.M. Budd, B.S. Ghanem, S. Makhseed, N.B. McKeown, K.J. Msayib, C.E. Tattershall, Chem. Commun. (2004) 230–231.
[21] S.C. Yan, Z.S. Li, Z.G. Zou, Langmuir 25 (2009) 10397–10401.
[22] D.W. Hwang, S. Lee, M. Seo, T.D. Chung, Anal. Chim. Acta 1033 (2018) 1–34.